



# Ferromagnetism of Mn-doped TiO<sub>2</sub> nanorods synthesized by hydrothermal method

S.K.S. Patel<sup>a</sup>, N.S. Gajbhiye<sup>a,\*</sup>, Sadgopal K. Date<sup>b</sup>

<sup>a</sup> Department of chemistry, Indian Institute of Technology Kanpur 208016, India

<sup>b</sup> Department of Physics, University of Pune, Pune 411007, India

## ARTICLE INFO

### Article history:

Received 22 July 2010

Received in revised form 14 January 2011

Accepted 18 January 2011

Available online 22 January 2011

### Keywords:

Room temperature ferromagnetism

Diluted magnetic semiconductor

Hydrothermal synthesis

Nanorod

## ABSTRACT

Mn-doped TiO<sub>2</sub> nanorods which showed room temperature ferromagnetic (RTFM) behavior have been synthesized by a hydrothermal method. Analysis of X-ray diffraction and Raman spectral data reveal the formation of anatase phase without any impurity phase. From the hysteresis loop measurements, it is possible to estimate the two parameters, magnetization ( $M_s$ ) and coercivity ( $H_c$ ) which are 33 memu/g and 89 Oe respectively, for 5 at% Mn-doped TiO<sub>2</sub>. The two parameters ( $M_s$ ,  $H_c$ ) are strongly dependent on the Mn doping concentration. The origin of the RTFM is understood in terms of the concentration of oxygen vacancies and/or defects which is created by Mn doping.

© 2011 Elsevier B.V. All rights reserved.

## 1. Introduction

Diluted magnetic semiconductors (DMSs) have provoked intense interest because semiconductors properties can be integrated with magnetic properties to realize the objective of fabrication of spin-based devices. For realizing practical spintronics devices, wide band gap diluted magnetic semiconductor system with large magnetic moments  $M$  and with a high Curie temperature  $T_c$  have attracted a great deal of attention [1–4]. ZnO and TiO<sub>2</sub> have been identified as a promising semiconductor material, exhibiting RTFM when doped with most of the transition metal elements [5–11].

Much of the focus of DMSs research has been towards substituting intrinsically magnetic metal ions into various semiconductors materials [12–14]. A drawback to this approach is that the dopant ions can segregate to form precipitates or clusters that are actually responsible for the ferromagnetic properties. The effect of such ferromagnetic clusters must be examined more carefully before the usefulness of such materials for spintronics applications can be determined [15]. In this context, recent reports [16–19] about the observation of RTFM in manganese doped TiO<sub>2</sub> has been taken with great enthusiasm by the scientific community. This is mostly because of the fact that the metallic manganese, as well as all possible Mn–O based secondary phases (except Mn<sub>3</sub>O<sub>4</sub> with  $T_c \sim 43$  K), are nonferromagnetic. So, if any FM behavior is observed at room

temperature (300 K) in a Mn-based system, then it will undoubtedly be the intrinsic property of the material [8,10].

In spite of the above interest, these studies have actually focused on the bulk materials and thin film, but the integration of DMS materials into electronics will need very low dimensions in order to make real use of the advantages offered by the spins. There is a tremendous current interest in the one-dimensional (1D) semiconductor nanostructures as well-defined building blocks to fabricate nanoscale electronic and optoelectronic devices [20,21]. In addition, realization of spintronic devices from the bottom up might be feasible by adopting the DMSs nanowires, nanotubes or nanorods. Therefore, to prepare 1D Mn-doped TiO<sub>2</sub> nanostructures through a simple method is important for both the physical research and potential applications of nanoscale spintronic devices.

In this article, we report a hydrothermal method to synthesize Mn-doped TiO<sub>2</sub> (Mn<sub>x</sub>Ti<sub>1-x</sub>O<sub>2</sub>) nanostructures with nanorod morphologies. Hysteresis loop ( $M$ – $H$ ) measurements were used to check the room temperature magnetic properties of the Mn-doped TiO<sub>2</sub> and all these results are presented in this paper.

## 2. Experimental details

TiO<sub>2</sub> nanorods were prepared using a chemical process similar to that described by Kasuga et al. [22,23]. In a typical preparation procedure, 1 g anatase TiO<sub>2</sub> white powders and stoichiometric amount of manganese nitrate Mn(NO<sub>3</sub>)<sub>2</sub>·4H<sub>2</sub>O were placed into a Teflon lined autoclave of 50 ml capacity. The autoclave was filled

\* Corresponding author. Tel.: +91 512 259 7423; fax: +91 512 259 7080.

E-mail address: [nsg@iitk.ac.in](mailto:nsg@iitk.ac.in) (N.S. Gajbhiye).

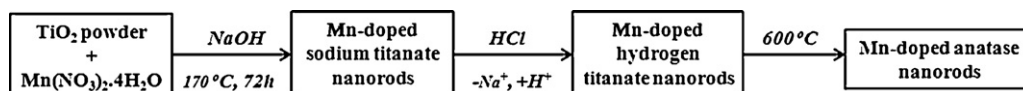


Fig. 1. Schematic representation of experimental procedure.

with 10 M NaOH aqueous solution up to 80% of the total volume, sealed into a stainless steel tank and maintained at 170 °C for 72 h without shaking or stirring during the heating. After that autoclave was naturally cooled to RT, the obtained precipitate Mn-doped sodium titanate was washed with H<sub>2</sub>O and filtered in the vacuum. Then Mn-doped sodium titanate was put into 500 mL of 0.1 N HCl aqueous solution at pH 2 and stirred for 24 h. This HCl treatment was repeated three times in order to exchange Na<sup>+</sup> ions completely by H<sup>+</sup> ions leading to the formation of Mn-doped hydrogen titanate nanorods. Then these Mn-doped hydrogen titanate nanorods were washed by distilled water until the pH reached to 7 and calcined in argon atmosphere at 600 °C for 4 h. At this temperature these nanorods were dehydrated and recrystallized into the Mn-doped anatase nanorods. The schematic representation of the experimental procedure is shown in Fig. 1.

The crystalline phases and their nature of the samples were determined by using a X-ray diffractometer (Thermo Electron Corporations, ARL X'TRA) with Cu K $\alpha$  radiation ( $\lambda = 1.5418 \text{ \AA}$ ). The crystal structure was further analyzed by Raman spectroscopy (Jobin Yvon Horiba iHR550). The morphologies of the sample were analyzed with field emission scanning electron microscopy (FESEM) (Quanta 200), and transmission electron microscopy (TEM) (Tecnai G<sup>2</sup>, operated at 200 kV). Hysteresis loop were measured at RT using vibrating sample magnetometer (DMS ADE-EV7 model).

### 3. Results and discussion

#### 3.1. Structural and morphological studies

XRD pattern of pure and doped anatase TiO<sub>2</sub> nanorods with different Mn concentration are shown in Fig. 2(a). It is revealed that diffraction peaks of the pure sample matches well with those of a standard anatase TiO<sub>2</sub> (JCPDS 21-1272). The Mn doping does not lead to the disappearance of the indexed peaks, proving that the crystallographic structure of the doped samples is similar to that of the pure anatase TiO<sub>2</sub> sample. No diffraction peaks from Mn related secondary phases such as MnO, Mn<sub>2</sub>O<sub>3</sub>, Mn<sub>3</sub>O<sub>4</sub> and MnO<sub>2</sub> were observed. The intensities of the characteristic strong peak (101), corresponding to anatase phase, decreased with increasing Mn concentration. In addition, compared with the pure TiO<sub>2</sub> nanorods, increasing Mn concentrations caused the slight shift in the peaks position of the doped TiO<sub>2</sub> to lower diffraction angles, as seen in the inset of Fig. 2(a) for the (101) peak. Furthermore it can be seen from Fig. 2(b) that the lattice parameters *c* increase monotonously with increasing Mn concentrations, the parameter *c* ranges from 9.4896 Å (for  $x = 0.00$ ) to 9.6046 Å (for  $x = 0.05$ ). This may be due to the fact that the ionic radii of Mn<sup>+2</sup> ions (0.80 Å) is larger than that of the Ti<sup>+4</sup> ions (0.68 Å), which suggest that the Mn ions are incorporated into the lattice of anatase TiO<sub>2</sub>.

The structural and morphological studies were carried out on these samples using FESEM and TEM. Mn-doped TiO<sub>2</sub> samples show the nanorods morphology having length around 0.2  $\mu\text{m}$  to several  $\mu\text{m}$  with a diameter around 50–90 nm (Fig. 3). It can be seen from selected area electron diffraction (SAED) patterns that only the diffraction related to the anatase TiO<sub>2</sub> phase was observed. It means that no Mn related secondary phases exist in the sample.

The phase formation and effect of Mn doping on the microstructural change in nanocrystalline material was further studied by Raman spectra. Anatase TiO<sub>2</sub> has a tetragonal structure (space group *I4<sub>1</sub>/amd*) with six Raman active modes: *A*<sub>1g</sub> (519 cm<sup>-1</sup>), *2B*<sub>1g</sub> (399 and 519 cm<sup>-1</sup>) and *3E*<sub>g</sub> (144, 197 and 639 cm<sup>-1</sup>) [24]. Fig. 4 shows the Raman spectra of the samples Mn<sub>*x*</sub>Ti<sub>1-*x*</sub>O<sub>2</sub> ( $0 \leq x \leq 0.05$ ). The peaks at  $\sim 144 \text{ cm}^{-1}$ ,  $\sim 399 \text{ cm}^{-1}$  and  $\sim 639 \text{ cm}^{-1}$  clearly demonstrate that all the samples are in pure anatase phase, in good agreement with the XRD results. The presence of any other vibration modes in the spectra was not detected. The low-frequency modes at *E*<sub>g</sub> (1) and those at *B*<sub>1g</sub> (1) are O–Ti–O bending type vibrations, and the modes at *E*<sub>g</sub> (3) and those at *A*<sub>1g</sub> (1) + *B*<sub>1g</sub> (2) are the Ti–O bond stretching type vibrations. The *E*<sub>g</sub> (1) and *E*<sub>g</sub> (3) modes are sensitive to the oxygen deficiency [25]. Due to Mn doping, the small extent of the structural distortion occurs, hence a moderate perturbation of the phonon states of the TiO<sub>2</sub> lattice can be expected. The coupling between TiO<sub>2</sub> lattice modes and vibrations of the Mn atoms may cause considerable changes in the Raman spectrum. It was observed that the most intense *E*<sub>g</sub> (1) (144 cm<sup>-1</sup>) peak of the undoped sample shows the blue shift, while the *E*<sub>g</sub> (3) (635 cm<sup>-1</sup>) peak is red shifted with increasing Mn concentration, indicating the increase of oxygen vacancies and/or

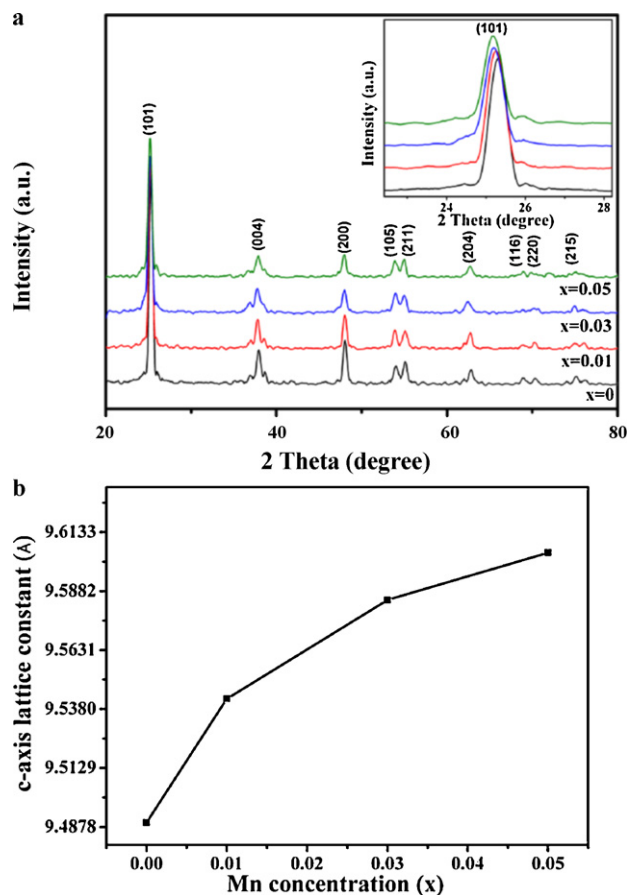


Fig. 2. (a) Powder X-ray diffraction patterns of different composition of Mn<sub>*x*</sub>Ti<sub>1-*x*</sub>O<sub>2</sub> ( $0 \leq x \leq 0.05$ ) and inset shows the broadening of the (101) peak. (b) Variation of the *c*-axis lattice parameters of Mn<sub>*x*</sub>Ti<sub>1-*x*</sub>O<sub>2</sub> with different Mn content ( $0 \leq x \leq 0.05$ ).

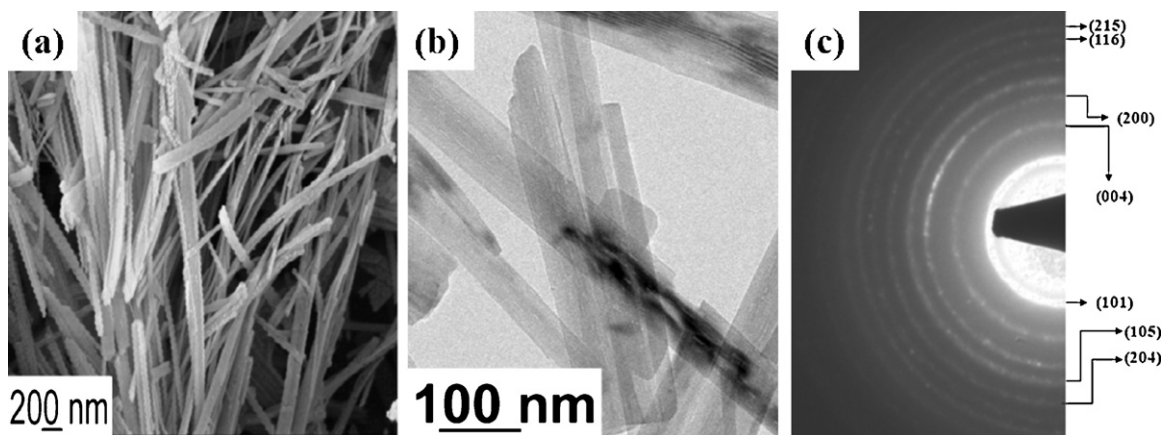


Fig. 3. Electron microscopic images and corresponding SAED pattern of  $\text{Mn}_{0.05}\text{Ti}_{0.95}\text{O}_2$  nanorods after annealing at  $600^\circ\text{C}$  (a) FESEM, (b) TEM and (c) SAED pattern.

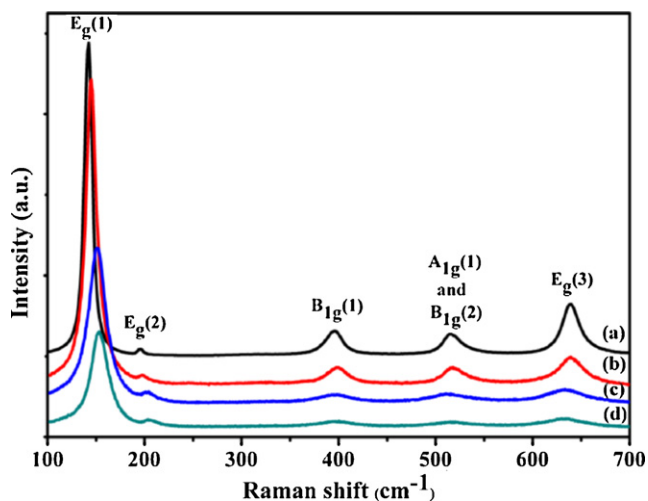


Fig. 4. Raman spectra of (a) undoped anatase and Mn-doped anatase nanorods, (b) 1 at.%, (c) 3 at.%, (d) 5 at.%.

defects formed via the substitution of Mn ions into titanium sites.

### 3.2. Magnetic studies

Hysteresis loops recorded at RT for the  $\text{Mn}_x\text{Ti}_{1-x}\text{O}_2$  nanorods with various Mn concentrations is shown in Fig. 5. The doped sample shows clear signature of ferromagnetism at RT, while the pure  $\text{TiO}_2$  nanorods show diamagnetism (in inset of Fig. 5). It is seen (Table 1) the magnetization and coercivity are 16, 24, 33 memu/g and 98, 98, 89 Oe for  $x=0.01, 0.03$  and  $0.05$ , respectively. It is significant and noteworthy to see that RTFM appeared even in 1 at.% Mn-doped  $\text{TiO}_2$  nanorods. In addition, magnetism in an undoped nonmagnetic hafnium dioxide has been attributed to oxygen vacancies [26].

The effect of the doping concentration on the origin of the RTFM can be explained by the bound magnetic polaron (BMP) model. According to the BMP model [27], the oxygen vacancies and defects

Table 1

The observed magnetization and coercivity for Mn-doped  $\text{TiO}_2$  at room temperature.

Sample (Mn (at.%))	Magnetization (memu/g)	Coercivity $H_c$ (Oe)
$\text{TiO}_2:\text{Mn}$ (1.0 at.%)	16	98
$\text{TiO}_2:\text{Mn}$ (3.0 at.%)	24	98
$\text{TiO}_2:\text{Mn}$ (5.0 at.%)	33	89

locally exist around magnetic ions and the magnetic  $\text{Mn}^{2+}$  ions substituted for  $\text{Ti}^{4+}$  sites in anatase like local environment. An electron is trapped in an oxygen vacancy. The donor electrons and magnetic impurities around it form BMP. The electrons associated with defects in oxides occupy large Bohr orbitals and form an impurity band. By allowing the impurity band to mix with the 3d state of Mn and to transfer a fraction of an electron for each vacancy, the 3d state would in turn polarize the impurity band and try to spread out sufficiently to overlap and interact with adjacent BMPs to realize the necessary ferromagnetic coupling, resulting the RTFM. Therefore, it seems that the appearance of a magnetic moment in the same doped samples may depend on the oxygen vacancies concentration (the doping concentration) and average distance between the  $\text{Mn}^{2+}-\text{Mn}^{2+}$  ions. As shown in Fig. 5, it is found that the value of the magnetization of the Mn-doped  $\text{TiO}_2$  nanorod increases with increasing the Mn concentration. This can be understood as the lower concentration of oxygen vacancies and longer  $\text{Mn}^{2+}-\text{Mn}^{2+}$  distances at low Mn concentration, favoring the lower number of overlapping polaron, as a result the ferromagnetic interaction is weak. When the Mn concentration reached 5 at.%, the higher concentration of oxygen vacancies increases the number of overlapping polaron and decreases the average distance between  $\text{Mn}^{2+}-\text{Mn}^{2+}$  ions, resulted ferromagnetic interaction between Mn ions is the strongest so that the higher  $M_s$  value 33 memu/g was obtained for the 5 at.% Mn-doped  $\text{TiO}_2$  nanorods.

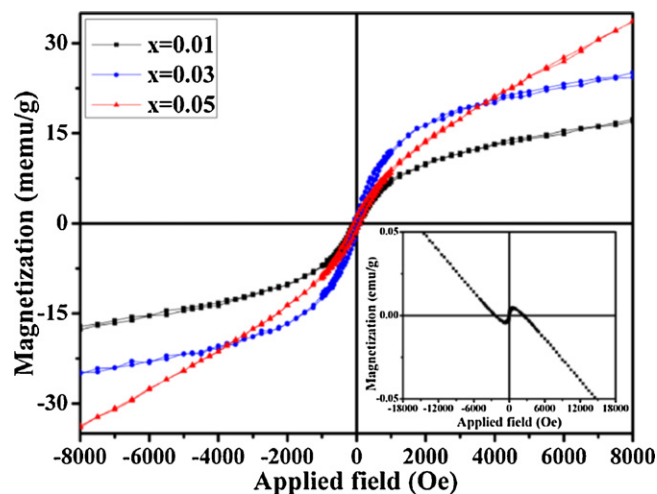


Fig. 5. Magnetic hysteresis loops ( $M-H$ ) at RT of  $\text{Mn}_x\text{Ti}_{1-x}\text{O}_2$  ( $0 \leq x \leq 0.05$ ) and inset shows the  $M-H$  loop of undoped  $\text{TiO}_2$ .

#### 4. Conclusions

In conclusion,  $Mn_xTi_{1-x}O_2$  nanorods with different Mn concentration have been successfully prepared by hydrothermal technique. The increase in Mn content leads to increase in *c*-axis lattice constant, which reveals  $Mn^{+2}$  ions as a substitution for  $Ti^{+4}$  ions in  $TiO_2$  crystal lattice without changing the tetragonal anatase structure. The Mn-doped  $TiO_2$  nanorods shows no indication of secondary phases such as MnO,  $MnO_2$  or  $Mn_2O_3$  clusters. The higher the concentration of oxygen vacancies and/or defects, the more the ferromagnetic domains coalesce, corresponding to higher magnetization. Therefore, the above discovery of the dependence of ferromagnetism is consistent with the description of ferromagnetism in the BMP model based on oxygen vacancies or/defects mechanism.

#### Acknowledgements

The authors acknowledge financial support from Department of Science and Technology (DST), India. One of the authors (S.K.S. Patel) thanks the Council of Scientific and Industrial Research (CSIR), New Delhi for the award of Senior Research Fellowship.

#### References

- [1] S.A. Wolf, D.D. Awschalom, R.A. Buhrman, J.M. Daughton, S. Vonmolnar, M.L. Roukes, A.Y. Chtchelkanova, D.M. Treger, *Science* 294 (2001) 1488.
- [2] A.P. Gary, *Science* 282 (1998) 1660.
- [3] T. Dietl, H. Ohno, F. Matsukura, J. Cibert, D. Ferrand, *Science* 287 (2000) 1019.
- [4] R. Janisch, P. Gopal, N.A. Spaldin, *J. Phys. Condens. Matter* 17 (2005) R657.
- [5] T.S. Herng, S.P. Lau, S.F. Yu, H.Y. Yang, L. Wang, M. Tanemura, J.S. Chen, *Appl. Phys. Lett.* 90 (2007) 032509.
- [6] H.S. Hsu, J.C.A. Huang, Y.H. Huang, Y.F. Liao, M.Z. Lin, C.H. Lee, J.F. Lee, S.F. Chen, L.Y. Lai, C.P. Liu, *Appl. Phys. Lett.* 88 (2006) 242507.
- [7] X.C. Liu, E.W. Shi, Z.Z. Chen, H.W. Zhang, B. Xiao, L.X. Song, *Appl. Phys. Lett.* 88 (2006) 252503.
- [8] M.H. Kane, K. Shalini, C.J. Summers, R. Varatharajan, J. Nause, C.R. Vestal, Z.J. Zhang, I.T. Ferguson, *J. Appl. Phys.* 97 (2005) 023906.
- [9] X. Liu, F. Lin, L. Sun, W. Cheng, X. Ma, W. Shi, *Appl. Phys. Lett.* 88 (2006) 062508.
- [10] Z.F. Wu, X.M. Wu, L.J. Zhuge, B. Hong, X.M. Yang, X.M. Chen, Q. Chen, *Mater. Lett.* 64 (2010) 472.
- [11] D. Karmakar, S.K. Mandal, R.M. Kadam, P.L. Paulose, A.K. Rajarajan, T.K. Nath, A.K. Das, I. Dasguptaand, G.P. Das, *Phys. Rev. B* 75 (2007) 144404.
- [12] N.J. Seong, S.G. Yoon, C.R. Cho, *Appl. Phys. Lett.* 81 (2002) 4209.
- [13] S. Ramachandran, A. Tiwari, J. Narayan, *Appl. Phys. Lett.* 84 (2004) 5255.
- [14] K.A. Griffin, A.B. Pakhomov, C.M. Wang, S.M. Heald, K.M. Krishnan, *Phys. Rev. Lett.* 94 (2005) 157204.
- [15] S.J. Pearton, W.H. Heo, M. Ivill, D.P. Norton, T. Steiner, *Semicond. Sci. Technol.* 19 (2004) R59.
- [16] J.P. Xu, J.F. Wang, Y.B. Lin, X.C. Liu, Z.L. Lu, Z.H. Lu, L.Y. Lv, F.M. Zhang, Y.W. Du, *J. Phys. D: Appl. Phys.* 40 (2007) 4757.
- [17] Z.M. Tian, S.L. Yuan, J.H. He, Y.Q. Wang, P. Li, H.Y. Xie, L. Liu, S.Y. Yin, *Solid State Commun.* 142 (2007) 545.
- [18] J.P. Xu, Y.B. Lin, Z.H. Lu, X.C. Liu, Z.L. Lu, J.F. Wang, W.Q. Zou, L.Y. Lv, F.M. Zhang, Y.W. Du, *Solid State Commun.* 140 (2006) 514.
- [19] L.M. Xu, X.J. Xing, M. Yang, X.Y. Li, S.X. Wu, P. Hu, J.Q. Lu, S.W. Li, *Appl. Phys. A* 98 (2010) 417.
- [20] D.S. Han, J. Park, K.W. Rhie, S. Kim, J. Chang, *Appl. Phys. Lett.* 86 (2005) 032506.
- [21] L.C. Tien, S.J. Pearton, D.P. Norton, F. Ren, *Appl. Phys. A* 91 (2008) 29.
- [22] T. Kasuga, M. Hiramatsu, A. Hoson, T. Sekino, K. Niihara, *Langmuir* 14 (1998) 3160.
- [23] T. Kasuga, M. Hiramatsu, A. Hoson, T. Sekino, K. Niihara, *Adv. Mater.* 11 (1999) 1307.
- [24] A.L. Bassi, D. Cattaneo, V. Russo, C.E. Bottani, E. Barborini, T. Mazza, P. Piseri, P. Milani, F.O. Ernst, K. Wegner, S.E. Pratsinis, *J. Appl. Phys.* 98 (2005) 074305.
- [25] H. Zhang, T. Ji, Y. Liu, J. Cai, *J. Phys. Chem. C* 112 (2008) 8604.
- [26] M. Venkatesan, C.B. Fitzgerald, J.M.D. Coey, *Nature* 430 (2004) 630.
- [27] A. Kaminiski, S.D. Sarma, *Phys. Rev. Lett.* 88 (2002) 247202.